Energy Efficiency of Commercial HVAC-based Virtual Batteries for Load Shifting

Weimin Wu, *Student Member, IEEE,* Shunbo Lei, *Senior Member, IEEE,* Qun Zhou Sun, *Member, IEEE,* and Johanna L. Mathieu, *Senior Member, IEEE*

***Abstract*—Commercial buildings with significant thermal inertia can be regarded as virtual batteries (VBs) when their heating, ventilation, and air conditioning (HVAC) systems participate in demand response. This is attributed to their battery-like feature of converting surplus (deficit) power into stored (released) cooling capacity, thereby reducing (increasing) future energy demand without compromising occupant comfort. An HVAC-based VB achieves the optimal efficiency when charging energy equals discharging energy, thereby avoiding additional energy consumption and ensuring mutual benefits of the grid and buildings. However, primary factors contributing to VB inefficiency remain unresolved, hindering VB development and applications. This work shows that the indoor temperature trajectory throughout a complete VB cycle is the key factor impacting HVAC-based VBs' additional energy consumption. We develop a method to quantify this impact based on a new concept, i.e., virtual leakage power. Furthermore, we derive the optimal efficiency condition, and propose an approach for quantifying the range of load shifting that a VB constrained by optimal efficiency can provide. Additionally, we design a model predictive control method for HVAC-based VBs to provide a specific amount of load shifting while ensuring optimal efficiency. Robustness of our results to assumptions made in the analysis is illustrated through simulation case studies.**

***Index Terms*—Commercial buildings, HVAC systems, demand flexibility, virtual battery, energy efficiency, ancillary services.**

NOMENCLATURE

Notation for Continuous-Time Analysis

t	Time
$T(t)$	Indoor temperature
$Q_{\text{heat}}(t)$	Heat transfer into building resulting from difference between $T(t)$ and T_{oa}
$Q_{\text{gain}}(t)$	Heat gain caused by internal loads and other weather factors other than T_{oa}
$P_{\text{hvac}}(t)$	HVAC system power consumption
$Q_{\text{hvac}}(t)$	Heat transfer due to HVAC system
$P_{\text{hvac}}^{\text{equ}}(T,t)$	Equilibrium power
$P_{\text{hvac}}^{\text{b}}(t)$	Baseline HVAC power
$COP_{\text{carnot}}(T)$	Inverse Carnot efficiency
$SoC(T(t))$	State of charge (SoC) of VB
$P_{\text{vb}}(t)$	Charging or discharging power of VB
$P_{\text{vb}}^{\text{change}}(t)$	Power to change current SoC
$P_{\text{vb}}^{\text{maintain}}(t)$	Power needed to maintain current SoC
$L(T,t)$	Virtual leakage power (VLP)

Additional Notation for Discrete-Time Analysis

τ	Time interval index
i	Index of stages (charging, discharging, and temperature recovery) in a VB cycle
T_τ	Indoor temperature at $t=\tau\cdot\Delta t$
$P_{\text{hvac},\tau}$	Average HVAC power in each time interval
L_τ	VLP at $t=\tau\cdot\Delta t$
ΔL_τ	Difference between L_τ and $L_{\tau-1}$
$\eta\vert_{T_{\tau-1}}^{T_\tau}$	An auxiliary variable
$P_{\text{vb},i}^{\text{mean}}$	Average VB power during i-th stage
L_i^{mean}	Mean $L(t)$ during i-th stage
F_{vb}	Load shifting flexibility of VB
E_{d}	Saved energy compared to the baseline during discharging stages
E_{c}	Absorbed energy compared to the baseline during charging stages
E_{hvac}	Total energy consumption of HVAC system during a complete VB cycle
E_{b}	Total baseline energy consumption
$P_{\text{hvac,cyc}}^{\text{b,mean}}$	Average baseline HVAC power during a complete VB cycle
$L_{\text{cyc}}^{\text{mean}}$	Average VLP during a complete VB cycle
T_τ^{mea}	Measured indoor temperature at $t=\tau\cdot\Delta t$
L_τ^{mea}	Measured VLP at $t=\tau\cdot\Delta t$
$\tilde{L}_\tau$	Predicted VLP at $t=\tau\cdot\Delta t$
$\tilde{T}_{\text{oa},\tau}$	Predicted outdoor temperature at $t=\tau\cdot\Delta t$
$\tilde{T}_\tau$	Predicted indoor temperature at $t=\tau\cdot\Delta t$
$\overline{T}_\tau$, $\underline{T}_\tau$	Bounds of T_τ
$\overline{L}_\tau$, $\underline{L}_\tau$	Bounds of VLP at $t=\tau\cdot\Delta t$
$\overline{\Delta L}_\tau$, $\underline{\Delta L}_\tau$	Bounds of ΔL_τ
$\overline{L}_i^{\text{mean}}$, $\underline{L}_i^{\text{mean}}$	Bounds of average VLP during i-th stage
$\overline{F}_{\text{vb}}$, $\underline{F}_{\text{vb}}$	Bounds of load shifting flexibility
$\boldsymbol{t_{\text{cyc}}}$	Set of time intervals in a complete VB cycle
$\mathcal{P}_{\text{var}}$	Set of time-varying values of HVAC power
$\mathcal{L}_{\text{var}}$	Set of time-varying values of VLP

This work was supported in part by the National Natural Science Foundation of China under Grant 52307145, in part by the Guangdong Basic and Applied Basic Research Foundation under Grants 2022A1515110833 and 2023A1515240051, and in part by the Shenzhen Science and Technology Program under Grant JCYJ20240813113532042. (*Corresponding author: S. Lei.*)

Weimin Wu and Shunbo Lei are with the School of Science and Engineering, The Chinese University of Hong Kong, Shenzhen, Guangdong 518172, China (e-mail: weiminwu@link.cuhk.edu.cn; leishunbo@cuhk.edu.cn).

Shunbo Lei is also with the Shenzhen Research Institute of Big Data, Shenzhen, Guangdong, 518172, China.

Qun Zhou Sun is with the Department of Electrical and Computer Engineering, University of Central Florida, Orlando, FL 32816, USA (e-mail: QZ.Sun@ucf.edu).

Johanna L. Mathieu is with the Department of Electrical Engineering and Computer Science, University of Michigan, Ann Arbor, MI 48109, USA (e-mail: jlmath@umich.edu).

Parameters for Analysis

s, f	Start/Final time of a demand response (DR) event
Δt	Length of each time interval
T_{oa}	Outdoor temperature
τ_i^{s}, τ_i^{f}	Start/Final time interval in i-th stage
$P_{\mathrm{hvac},i}^{\mathrm{b,mean}}$	Mean $P_{\mathrm{hvac}}^{b}(t)$ during i-th stage
R	Building thermal resistance
C	Building thermal capacity
M	Mass of indoor air
$T^{\min}$, $T^{\max}$	Min/Max allowed indoor temperature
T_{b}	Baseline indoor temperature setpoint
n_{cyc}	Total number of time intervals
n_i	Total number of time intervals in i-th stage
T_i^{set}	Indoor temperature setpoint in i-th stage
$P_{\mathrm{hvac}}^{\min}$, $P_{\mathrm{hvac}}^{\max}$	Min/Max HVAC power consumption

Additional Parameters for Simulation

β	Damper position
C_{w}	Wall thermal capacity
R_1	Thermal resistance between wall and thermal zone
R_2	Thermal resistance between wall and outdoors
c_{air}	Specific heat capacity of air
T_{sa}	Supply air temperature

I. Introduction

With the increasing penetration of variable renewable energy sources in power systems, more ancillary services resources are needed to rectify supply-demand mismatch in real time. Heating, ventilation, and air conditioning (HVAC) systems in commercial buildings are ideal ancillary services providers [1]–[3], as they can vary their power demand up and down around their baseline, and quality of service can be maintained owing to their large thermal energy capacity and thermal inertia [4]. To the grid, they exhibit battery-like characteristics and can be thought of as virtual batteries (VBs) [5]–[8].

Energy efficiency is a critical issue for HVAC-based VBs, as perturbations are introduced to well-functioning building controls, affecting the total energy consumption relative to the baseline, i.e., the power consumption would have occurred if the building had not provided demand response (DR). The extra energy is a cost of control to the asset owner and should be factored into the cost of providing DR [9]. Round-trip efficiency (RTE), which is the ratio of discharging energy to charging energy, and additional energy consumption (AEC), which is the sum of charging and discharging energy, are commonly employed metrics to evaluate the efficiency of HVAC-based VBs [9]–[11]. Note that in this work, $\mathrm{RTE} = 1$ (i.e., $\mathrm{AEC} = 0$) is considered as the optimal VB efficiency. Although cases with discharging energy larger than charging energy (i.e., $\mathrm{RTE} > 1$ and $\mathrm{AEC} < 0$) is efficient from an energy conservation perspective, they might significantly impact building occupants' comfort, which should also be factored into the cost of providing DR. For example, simulations in [12] show that, in summer cooling mode, an HVAC-based VB with $\mathrm{RTE} = 1$ would result in a slight increase in the average indoor temperature during DR compared to the baseline situation. When $\mathrm{RTE} > 1$, the average indoor temperature increase will be even larger, as less energy is supplied for building cooling. Conversely, when $\mathrm{RTE} < 1$ (i.e., $\mathrm{AEC} > 0$), buildings have extra cost associated with the additional consumption of energy. Therefore, in this work, values of RTE (respectively, AEC) less than or greater than 1 (respectively, 0) are considered undesirable and failing to serve mutual interests of the grid and buildings.

Energy inefficiency, indicated by $\mathrm{RTE} < 1$ and $\mathrm{AEC} > 0$, has been reported in many works on HVAC-based VB experiments. The authors of [9] conducted experiments by applying a DR control strategy proposed in [13] to a $30000\ \mathrm{m}^2$ building at Los Alamos National Laboratory. It was observed that the DR actions produced positive AEC in almost all experiments, and the average RTE was less than 0.5. Such energy inefficiency has been shown to generally exist in HVAC-based VBs. In the experiments reported in [10] and [11], adjusting thermostat setpoints in several buildings on university campuses resulted in a shift in HVAC power consumption. The observed RTE values range from 0.34 to 0.81, indicating unsatisfactory efficiency in most tests. In [14], [15], the authors reported experimental results from Lawrence Berkeley National Laboratory's Facility for Low Energy eXperiments (FLEXLAB), which showed a slight increase in energy consumption in some cases compared to the baseline and the average indoor temperature was observed to drop by $1 \sim 2\ ^{\circ}\mathrm{C}$.

The above reported experiments and analyses have implied an unexplored relationship between HVAC-based VB efficiency and indoor temperature trajectories (which was simply quantified by the average indoor temperature in related works). These studies also show that the efficiency of a VB is variable, and there is no known method to ensure the optimal efficiency with $\mathrm{RTE} = 1$ and $\mathrm{AEC} = 0$. Therefore, the aim of this work is to explore the indoor temperature trajectory-dependent characteristic of HVAC-based VB efficiency and develop a method to improve the efficiency.

In the past few years, scholars have been trying to identify factors that impact the efficiency of HVAC-based VBs and explore efficiency-enhancing methods. Ref. [7] attributes the inefficiency to building physics (state-dependent energy losses, etc., which lead to actual additional energy consumption), and inaccurate measurements (biased baseline estimates, etc., which lead to errors in efficiency quantification). Ref. [16] develops a physics-based simulation model, within which the thermostatic control system utilizes a PI controller, to simulate HVAC power variation during load shifting DR events. It reports RTE ranging from 0.81 to 0.94 for pre-cooling events (i.e., virtual charging first, and then virtual discharging), and 1.05 to 1.19 for post-cooling events (i.e., virtual discharging first, and then virtual charging). It finds that the RTE is related to building parameters, control design, and baseline model accuracy. To enhance the efficiency, [17] finds that faster time-scale ancillary services leads to smaller impact on HVAC energy consumption while still maintaining a comfortable indoor climate. In [18], the authors conduct a simulation-based

analysis in which the VB power is simplified to a square wave (i.e., a charging window immediately followed by a discharging window, or the other way around, with the same power magnitude and duration) to provide DR service and required energy for building temperature recovery. It is proved that when the square wave of HVAC power is repeated n times, in the limit where $n \to \infty$, the asymptotic RTE is 1. In another work [12], the same authors discussed the relationship between the average indoor temperature and RTE, but did not explore how the indoor temperature trajectory affects the efficiency as we do here.

In general, although there is still no consistent consensus regarding factors affecting HVAC-based VB efficiency (as also noted in [7]), scholars have realized the unexplored relationship between VB efficiency and indoor temperature trajectories through experiments [14], [15] and simulations [12]. Therefore, this paper endeavors to reveal the indoor temperature trajectory-dependent characteristic of VB efficiency and to quantify this effect based on thermodynamic analysis.

In short, this work introduces a new concept, *virtual leakage power*, to capture the influence of the indoor temperature trajectory on HVAC-based VB efficiency, and derives the condition and flexibility range associated with the VB's optimal efficiency. This work also proposes a model predictive control (MPC) method to enhance VB efficiency. The main contributions are summarized as follows:

- *Derive the optimal efficiency condition for HVAC-based VBs:* We show that the indoor temperature trajectory throughout a complete VB cycle is a key factor influencing a VB's efficiency. A novel concept termed *virtual leakage power (VLP)*, which can be utilized to calculate AEC directly, is proposed for quantifying the influence. Furthermore, we deduce that for the VB to perfectly balance the charging and discharging energy (i.e., achieve the optimal efficiency), the integrals of VLP and baseline HVAC power must be equal.
- *Load shifting flexibility range quantification and a control method to provide a specific amount of flexibility:* We define the flexibility of a HVAC-based VB as the average charging/discharging energy and develop a method to evaluate the flexibility range of a VB constrained by the optimal efficiency condition. We also propose an MPC approach to control the HVAC-based VB and provide a specific amount of flexibility while meeting the optimal efficiency condition.
- *Verify robustness of the theoretical analysis and proposed methods to assumptions:* We conduct simulations using an HVAC-based VB model that is more practical and detailed than the one utilized in our theoretical analysis, and the assumptions are relaxed. Numerical results show that the average error of AEC calculated using the proposed VLP based method is 0.018%. The proposed MPC controller effectively enables load shifting of HVAC-based VBs while keeping $\mathrm{RTE} = 1 \pm 0.0001$. That is, the simulation results validate the robustness and applicability of our analysis and methods.

The rest of this paper is organized as follows. Section II models the HVAC-based VB, and discusses the new concept of VLP and how the indoor temperature trajectory affects VB efficiency. Section III quantifies the influence of indoor temperature trajectories on VB efficiency and provides a mathematical derivation of the optimal VB efficiency condition. Section IV presents a method to quantify the optimal efficiency-constrained VB flexibility range. Section V proposes an MPC approach for HVAC-based VBs to provide a specific amount of load shifting. In Section VI, the robustness of our analysis and proposed approaches are illustrated through numerical simulations. Conclusions are provided in Section VII.

II. Modeling of HVAC-based Virtual Batteries and Virtual Leakage Power

This section models a commercial building and its HVAC system as a VB, and briefly discusses potential factors that may influence VB efficiency. Without loss of generality, HVAC systems are assumed to operate in cooling mode in this paper.

A. Thermodynamics Modeling of an HVAC-based VB

The resistor-capacitor (RC) model is widely used to describe the thermodynamics of a commercial building with an HVAC system [12], [18]–[20]. It can be expressed as follows:

$$\frac{dT}{dt} = \frac{1}{M \cdot C} \cdot [Q_{\mathrm{heat}}(T(t)) + Q_{\mathrm{gain}}(t) - Q_{\mathrm{hvac}}(t)] \quad (1)$$

$$Q_{\mathrm{heat}}(T(t)) = \frac{1}{R} \cdot (T_{\mathrm{oa}} - T(t)) \quad (2)$$

$$Q_{\mathrm{hvac}}(t) = COP(T(t)) \cdot P_{\mathrm{hvac}}(t) \quad (3)$$

where R represents the building structure's thermal resistance, C represents the building's thermal capacitance, $T(t)$ is the indoor temperature which is a function of time, M is the mass of indoor air, $Q_{\mathrm{heat}}(T(t))$ represents the exogenous heat transfer into the building resulting from the difference between $T(t)$ and the outdoor temperature T_{oa}, $Q_{\mathrm{gain}}(t)$ is the heat gain caused by internal loads and other weather factors except outdoor temperature, $Q_{\mathrm{hvac}}(t)$ is the heat transfer due to the HVAC system, $COP(T(t))$ is the cooling system's coefficient of performance which depends on $T(t)$, and $P_{\mathrm{hvac}}(t)$ is the HVAC system power consumption. Several assumptions are made:

Assumption 1: Parameters M, C, and R are assumed to be constants, given their negligible variations under building cooling conditions [20].

Assumption 2: T_{oa} is assumed to be constant during a short-term DR event. (This is a common assumption in theoretical analysis of HVAC-based VB energy efficiency, e.g., see [12], [16], [18]. It also makes our derivations more clear. We will relax this assumption in our case studies to verify the robustness of our results.)

Assumption 3: To analyze the theoretical efficiency of the HVAC-based VB, we assume that the COP is determined by the inverse Carnot efficiency (COP_{carnot}), which represents the maximum theoretically-achievable efficiency according to thermodynamics principles [20]. The value of COP_{carnot} varies with the indoor temperature $T(t)$:

$$COP_{\mathrm{carnot}}(T(t)) = \frac{T(t)}{T_{\mathrm{oa}} - T(t)}. \quad (4)$$

The following terms are also defined to model VBs [18], [12].

Definition 1 (Charging/Discharging Power): For the external grid, an increase or decrease of HVAC power consumption $P_{\mathrm{hvac}}(t)$ with respect to the baseline power $P^{\mathrm{b}}_{\mathrm{hvac}}(t)$ can be seen as charging and discharging, respectively. Thus, we define $P_{\mathrm{vb}}(t)$, the deviation of HVAC power from the baseline power, as the VB's charging or discharging power:

$$P_{\mathrm{vb}}(t) = P_{\mathrm{hvac}}(t) - P^{\mathrm{b}}_{\mathrm{hvac}}(t), \tag{5}$$

where a positive value indicates a charging power, and a negative value indicates a discharging power. The baseline power $P^{\mathrm{b}}_{\mathrm{hvac}}(t)$ will be discussed in the following section.

Definition 2 (State of Charge (SoC) of HVAC-based VBs): An HVAC-based VB operates by increasing/decreasing its electricity consumption to decrease/increase building indoor temperature, which also changes later electricity consumption owing to the building's significant thermal inertia. Thus, given the allowed indoor temperature range $[T^{\min}, T^{\max}]$, the SoC for an HVAC-based VB can be defined as follows [18]:

$$SoC(T(t)) = \frac{T^{\max} - T(t)}{T^{\max} - T^{\min}}. \tag{6}$$

Definition 3 (Complete VB Cycle): An HVAC-based VB has undergone a complete cycle from start time s to final time f, if $SoC(T(s)) = SoC(T(f)) = SoC(T_{\mathrm{b}})$, where T_{b} is the baseline temperature setpoint. The period $\boldsymbol{t_{cyc}} = [s, f]$ is called a complete VB cycle. The period $\boldsymbol{t_{cyc}}$ can be divided into two parts, i.e., the charging time $\boldsymbol{t_c}$ and the discharging time $\boldsymbol{t_d}$ ($\boldsymbol{t_{cyc}} = \boldsymbol{t_c} \cup \boldsymbol{t_d}$). There are no requirements on the lengths, sequences, or times of charge/discharge during a complete VB cycle.

B. Energy Efficiency Metrics of HVAC-based VBs

Next we can introduce two commonly used metrics to evaluate the efficiency of HVAC-based VBs. First, the round-trip efficiency (RTE) is defined as [12], [16], [18]:

$$\mathrm{RTE} = \frac{E_{\mathrm{d}}}{E_{\mathrm{c}}} = \frac{-\int_{t\in\boldsymbol{t_d}} P_{\mathrm{vb}}(t)\cdot dt}{\int_{t\in\boldsymbol{t_c}} P_{\mathrm{vb}}(t)\cdot dt}, \tag{7}$$

where E_{d} represents the saved energy compared to the baseline during discharging stages, and E_{c} is the absorbed energy compared to the baseline during charging stages.

Another metric is the additional energy consumption (AEC) [7], [10], [11], which measures the HVAC system's increased energy consumption compared with its baseline:

$$\mathrm{AEC} = \int_{t\in\boldsymbol{t_{cyc}}} P_{\mathrm{vb}}(t)\cdot dt. \tag{8}$$

The formulation of AEC offers greater convenience for energy efficiency analysis and derivations in this work, as it eliminates the need to distinguish between charging and discharging stages. As mentioned in Section I, considering both energy conservation and building occupant comfort, we consider $\mathrm{AEC} = 0$ (i.e., $\mathrm{RTE} = 1$) as the optimal efficiency of HVAC-based VBs.

C. Dependence of VB Power on the Temperature Trajectory

As mentioned in Section I, there is a correlation between the efficiency of HVAC-based VBs and the trajectory of indoor temperature. However, a mathematical explanation is still lacking. In this subsection, we first explore how indoor temperature trajectory affects VB power (i.e., the influence of both $T(t)$ and dT/dt on $P_{\mathrm{vb}}(t)$), since the AEC is calculated by integrating $P_{\mathrm{vb}}(t)$ as shown in (8).

Based on Assumptions 1-3 and substituting (3) into (1), we obtain the relationship between the HVAC power consumption and the building's thermodynamics:

$$P_{\mathrm{hvac}}(t) = \frac{-M\cdot C\cdot \frac{dT}{dt}}{COP_{\mathrm{carnot}}(T(t))} + \frac{Q_{\mathrm{heat}}(T(t)) + Q_{\mathrm{gain}}(t)}{COP_{\mathrm{carnot}}(T(t))}. \tag{9}$$

To derive the condition for an HVAC system to reach its equilibrium state (maintaining the indoor temperature at a fixed value), we set $dT/dt = 0$ and substitute (2) and (4) into (9) to obtain:

$$P^{\mathrm{equ}}_{\mathrm{hvac}}(T,t) = \frac{\left(T_{\mathrm{oa}} - T(t)\right)^2}{R\cdot T(t)} + \frac{T_{\mathrm{oa}} - T(t)}{T(t)}\cdot Q_{\mathrm{gain}}(t). \tag{10}$$

This means that the HVAC system needs to consume the equilibrium power, $P^{\mathrm{equ}}_{\mathrm{hvac}}(T,t)$, to maintain the current indoor temperature. As shown in (10), the equilibrium power depends on the indoor temperature $T(t)$ (or the SoC) and $Q_{\mathrm{gain}}(t)$.

Based on (2) and (10), the equilibrium power is equal in quantity to the power required to counterbalance $Q_{\mathrm{heat}}(T(t))$ and $Q_{\mathrm{gain}}(t)$ at time t. In other words, there is a portion of the electricity charged into the VB that is not used to change the SoC but rather consumed to counteract the natural loss (similar to the leakage of a traditional battery). Therefore, we define a new concept termed *virtual leakage power* (*VLP*) for HVAC-based VBs.

Definition 4 (Virtual Leakage Power): We define $L(T,t)$ as an HVAC-based VB's VLP at time t when the indoor temperature is T, which can be determined by:

$$L(T,t) = P^{\mathrm{equ}}_{\mathrm{hvac}}(T,t). \tag{11}$$

Additionally, the baseline power of an HVAC-based VB can be defined as the VLP at the baseline temperature setpoint [18].

Definition 5 (Baseline Power): The baseline power $P^{\mathrm{b}}_{\mathrm{hvac}}(t)$ is the power consumed to maintain the baseline temperature setpoint T_{b}:

$$P^{\mathrm{b}}_{\mathrm{hvac}}(T_{\mathrm{b}},t) = \frac{\left(T_{\mathrm{oa}} - T_{\mathrm{b}}\right)^2}{R\cdot T_{\mathrm{b}}} + \frac{T_{\mathrm{oa}} - T_{\mathrm{b}}}{T_{\mathrm{b}}}\cdot Q_{\mathrm{gain}}(t), \tag{12}$$

which varies according to changes in $Q_{\mathrm{gain}}(t)$.

With the introduction of VLP, (5) can be modified to:

$$P_{\mathrm{vb}}(t) = \frac{-M\cdot C\cdot \frac{dT}{dt}}{COP_{\mathrm{carnot}}(T(t))} + L(T,t) - P^{\mathrm{b}}_{\mathrm{hvac}}(T_{\mathrm{b}},t). \tag{13}$$

From the perspective of conservation of energy, the real-time charging/discharging power $P_{\mathrm{vb}}(t)$ of an HVAC-based VB is composed of $P^{\mathrm{change}}_{\mathrm{vb}}(t)$, the power to change the current

This article has been accepted for publication in IEEE Transactions on Power Systems. This is the author's version which has not been fully edited and content may change prior to final publication. Citation information: DOI 10.1109/TPWRS.2025.3596899

SoC, and $P_{\rm vb}^{\rm maintain}(t)$, the power to maintain the current SoC, i.e.,

$$P_{\rm vb}(t) = P_{\rm vb}^{\rm change}(t) + P_{\rm vb}^{\rm maintain}(t), \tag{14a}$$

$$P_{\rm vb}^{\rm change}(t) = \frac{-M \cdot C \cdot \frac{dT}{dt}}{COP_{\rm carnot}(T(t))}, \tag{14b}$$

$$P_{\rm vb}^{\rm maintain}(t) = L(T,t) - P_{\rm hvac}^{\rm b}(T_{\rm b},t). \tag{14c}$$

Both $P_{\rm vb}^{\rm change}(t)$ and $P_{\rm vb}^{\rm maintain}(t)$ can be positive, negative, or zero. As indicated in (14b), $P_{\rm vb}^{\rm change}(t)$ is primarily influenced by the rate of change of indoor temperature, dT/dt, since the variation in $COP_{\rm carnot}$ within the indoor temperature comfort range is relatively small [16], [18]. In contrast, according to (10), (11), and (14c), $P_{\rm vb}^{\rm maintain}(t)$ depends on $T(t)$. A visual representation of these relationships is provided in Fig. 1. As shown, the sign of $P_{\rm vb}^{\rm change}(t)$ (green line in Fig. 1(b)) is opposite that of dT/dt (red line in Fig. 1(c)). Similarly, the rate of change of $P_{\rm vb}^{\rm maintain}(t)$, denoted $dP_{\rm vb}^{\rm maintain}(t)/dt$ (orange line in Fig. 1(c)), exhibits an inverse relationship with dT/dt. Consequently, the integral values of these power components are determined by the indoor temperature trajectory. As indicated by (7) and (8), the VB efficiency is a function of the integrals of charging and discharging power throughout a complete VB cycle. Therefore, it can be inferred that the efficiency of a VB is affected by the temperature trajectory. The following analysis will quantify this effect and provide the condition for achieving the optimal VB efficiency.

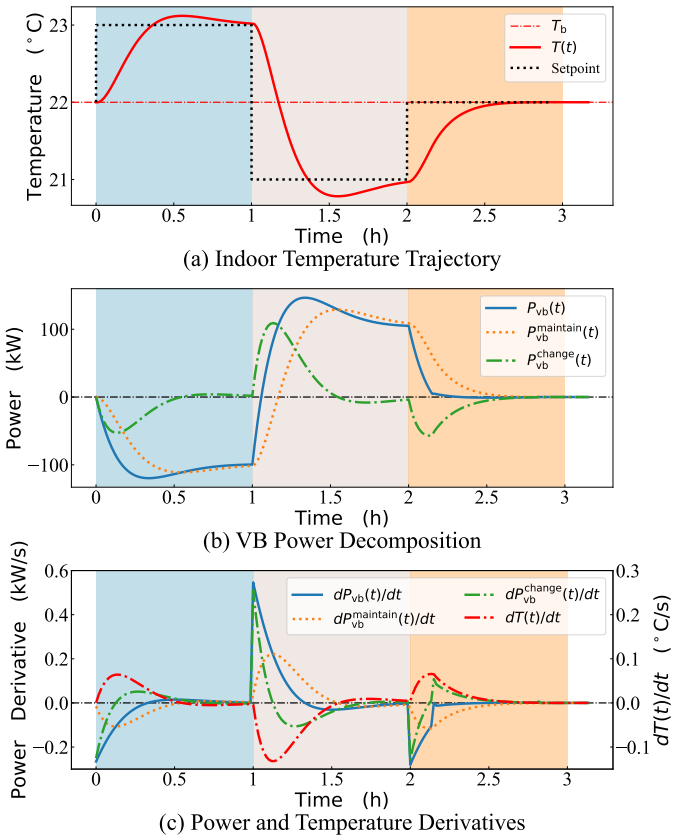

(a) Indoor Temperature Trajectory

(b) VB Power Decomposition

(c) Power and Temperature Derivatives

Fig. 1. An illustration of the relationship between $P_{\rm vb}(t)$, $P_{\rm vb}^{\rm change}(t)$, and $P_{\rm vb}^{\rm maintain}(t)$. In this example, RTE $= 0.88$, AEC $= 13.69$ kWh, $\int P_{\rm vb}^{\rm maintain}(t)\cdot dt = 13.69$ kWh, and $\int P_{\rm vb}^{\rm change}(t)\cdot dt = 0.00$ kWh.

III. Analytical Analysis of the Efficiency of HVAC-based Virtual Batteries

A. Influence of Indoor Temperature Trajectory on AEC

As shown by (7) and (8), the efficiency can be evaluated from the known HVAC power variation throughout a complete VB cycle. The power variation depends on the indoor temperature trajectory $T(t)$, which is influenced by external perturbations (e.g., $Q_{\rm gain}(t)$), setpoint changes, and the used control strategy. Researchers often make simplifications by assuming fixed power changes (e.g., square-wave HVAC power consumption in [12] and [18]) or fixed control strategies (e.g., PI controller with no external perturbations in [16]).

Additionally, in all existing relevant analyses (e.g., [12], [16], [18]), specific indoor temperature trajectories are explicitly or implicitly assumed. As mentioned in Section II, the efficiency of HVAC-based VBs highly depends on the temperature trajectory. Thus, analyses relaxing such assumptions are needed to attain results that are robust against different control strategies, setpoint changes, and external perturbations.

In this work, we do not assume specific HVAC power variations or indoor temperature trajectories. This will help to improve the generality of our AEC analysis and derivation. Specifically, using numerical integration, we calculate and accumulate the approximated integrals of $P_{\rm vb}(t)$ over subintervals within a complete cycle of HVAC-based VBs.

First, the entire integral domain $\boldsymbol{t_{\rm cyc}}$ is divided into N subintervals, where N is an infinitely large positive integer. Thus, let $\{t_\tau\}$ be a partition of $[s,f]$ with regular spacing (i.e., $s = t_0 < t_1 < \cdots < t_\tau < \cdots < t_{N-1} < t_N = f$). Then, we obtain:

$$\text{AEC} = \int_s^f P_{\rm vb}(t)\cdot dt = \sum_{\tau=1}^{N}\int_{t_{\tau-1}}^{t_\tau} P_{\rm vb}(t)\cdot dt. \tag{15}$$

The next step is to find a quantity ΔE_τ to approximate $\int_{t_{\tau-1}}^{t_\tau} P_{\rm vb}(t)\cdot dt$ such that $\int_s^f P_{\rm vb}(t)\cdot dt \approx \sum_{\tau=1}^{N}\Delta E_\tau$ [21]. We use the trapezoidal integration, to construct ΔE_τ. The error caused by this approximate integration method has been proven to be sufficiently small for $N\to\infty$ [22]. Thus, based on (13), we have:

$$\begin{aligned}
&\int_{t_{\tau-1}}^{t_\tau} P_{\rm vb}(t)\cdot dt \\
&= \int_{t_{\tau-1}}^{t_\tau} \frac{-M\cdot C\cdot\frac{dT}{dt}}{COP_{\rm carnot}(T(t))}\cdot dt + \int_{t_{\tau-1}}^{t_\tau}\left[L(t) - P_{\rm hvac}^{\rm b}(t)\right]\cdot dt \\
&\approx -M\cdot C\cdot \eta\big|_{T_{\tau-1}}^{T_\tau} + \int_{t_{\tau-1}}^{t_\tau}\left[L(t) - P_{\rm hvac}^{\rm b}(t)\right]\cdot dt = \Delta E_\tau,
\end{aligned} \tag{16}$$

where $T_{\tau-1}$ and T_τ are the indoor temperatures at $t_{\tau-1}$ and t_τ, respectively, and $\eta\big|_{T_{\tau-1}}^{T_\tau}$ serves as an auxiliary variable to simplify the expression:

$$\eta\big|_{T_{\tau-1}}^{T_\tau} = T_{\rm oa}\cdot\ln\frac{T_\tau}{T_{\tau-1}} - (T_\tau - T_{\tau-1}). \tag{17}$$

A more detailed derivation of (16)-(17) is provided in our online appendix [23].

Based on (15) and (16), and assuming an indoor temperature trajectory with both an initial temperature and final temperature associated with a complete VB cycle of $T_{\rm b}$ (see *Definition* 3), the AEC can be further expressed as:

$$\begin{aligned}\mathrm{AEC} = &- M\cdot C\cdot \sum_{\tau=1}^{N}\eta|_{T_{\tau-1}}^{T_\tau} \\ &+\sum_{\tau=1}^{N}\int_{t_{\tau-1}}^{t_\tau}\left[L(t)-P_{\rm hvac}^{\rm b}(t)\right]\cdot dt, \\ &T_0 \;=\; T_N \;=\; T_{\rm b}.\end{aligned} \tag{18}$$

Substituting (17) into (18), the first term of the right side of (18) is shown to be zero:

$$\begin{aligned}-M\cdot C\cdot\sum_{\tau=1}^{N}\eta|_{T_{\tau-1}}^{T_\tau} &= -M\cdot C\cdot\left[T_{\rm oa}\cdot\ln\frac{T_N}{T_0}-(T_N-T_0)\right] \\ &= -M\cdot C\cdot\left[T_{\rm oa}\cdot\ln\frac{T_{\rm b}}{T_{\rm b}}-(T_{\rm b}-T_{\rm b})\right]=0\end{aligned} \tag{19}$$

Then (18) is reduced to:

$$\mathrm{AEC}=\sum_{\tau=1}^{N}\int_{t_{\tau-1}}^{t_\tau}\left[L(t)-P_{\rm hvac}^{\rm b}(t)\right]\cdot dt,\ T_0=T_N=T_{\rm b}, \tag{20}$$

and based on (14b), (16), (17) and (19), we have:

$$\int\limits_{t\in\boldsymbol{t_{cyc}}} P_{\rm vb}^{\rm change}(t)\cdot dt=\int\limits_{t\in\boldsymbol{t_{cyc}}}\frac{-M\cdot C\cdot\frac{dT}{dt}}{COP_{\rm carnot}(T(t))}\cdot dt=0. \tag{21}$$

This implies that, although $COP_{\rm carnot}(T(t))$ is not constant (as indicated by (4), which shows that HVAC systems consume less power at high indoor temperatures than at low indoor temperatures to provide the same cooling capacity), its temperature-dependent variation has no direct effect on VB efficiency, which is also illustrated in Fig. 1.

Thus, based on (14c), and substituting (10) and (11) into (20), we obtain:

$$\begin{aligned}\mathrm{AEC} &= \int\limits_{t\in\boldsymbol{t_{cyc}}} P_{\rm vb}^{\rm maintain}(t)\cdot dt \\ &= \int\limits_{t\in\boldsymbol{t_{cyc}}}\left[L(T(t),t)-P_{\rm hvac}^{\rm b}(T_{\rm b},t)\right]\cdot dt \\ &= \int\limits_{t\in\boldsymbol{t_{cyc}}}\left[\begin{array}{c}\left(\frac{T_{\rm oa}^2}{R}+T_{\rm oa}\cdot Q_{\rm gain}(t)\right)\cdot\left(\frac{1}{T(t)}-\frac{1}{T_{\rm b}}\right)\\ +\frac{1}{R}\cdot(T(t)-T_{\rm b})\end{array}\right]\cdot dt.\end{aligned} \tag{22}$$

As indicated by the third line of (22), in a complete VB cycle, the indoor temperature trajectory $T(t)$ is the only internally controllable factor impacting VB efficiency, as all other parameters are fixed or externally determined. As indicated by the second line of (22), the influence of the indoor temperature trajectory on the AEC can be quantified by integrating the difference between the temperature-dependent VLP and the baseline HVAC power.

B. Condition to Achieve the Optimal VB Efficiency

The condition for an HVAC-based VB to achieve the optimal efficiency can be derived by setting $\mathrm{AEC}=0$ in (22). By introducing

$$L_{\rm cyc}^{\rm mean}=\frac{\int_s^f L(T(t),t)\cdot dt}{(f-s)} \tag{23}$$

to represent the average VLP during $[s,f]$, and

$$P_{\rm hvac,cyc}^{\rm b,mean}=\frac{\int_s^f P_{\rm hvac}^{\rm b}(T_{\rm b},t)\cdot dt}{(f-s)} \tag{24}$$

to represent the average baseline HVAC power during $[s,f]$, the optimal VB efficiency condition can be represented as:

$$L_{\rm cyc}^{\rm mean}=P_{\rm hvac,cyc}^{\rm b,mean}. \tag{25}$$

In general, the condition for an HVAC-based VB to achieve the optimal efficiency (i.e., $\mathrm{AEC}=0$ and $\mathrm{RTE}=1$) is that the difference between the integrals of VLP and baseline power throughout the complete VB cycle equals zero. To simplify the expression for practical engineering applications, we express this condition as their respective means being equal (i.e., (25)).

As shown in (14), the VB power $P_{\rm vb}(t)$ is determined by dT/dt and $T(t)$, also indicating impacts of the indoor temperature trajectory on the HVAC power variation. Therefore, by designing a specific indoor temperature trajectory that meets (25) and controlling the HVAC system according to this temperature trajectory, an optimal efficiency-constrained VB, which also can provide specific power variations, can be attained. More details are given in Sections IV and V.

C. Energy Inefficiency of Violating the Optimal Condition

The impact of failing to meet the above optimal VB efficiency condition should also be analyzed to evaluate the efficiency loss associated with unconstrained indoor temperature trajectories. We first define the *leakage deviation ratio (LDR)* to quantify the deviation between the average VLP and average baseline HVAC power:

$$\mathrm{LDR}=\frac{\int_s^f L(T(t),t)\cdot dt}{\int_s^f P_{\rm hvac}^{\rm b}(T_{\rm b},t)\cdot dt}=\frac{L_{\rm cyc}^{\rm mean}}{P_{\rm hvac,cyc}^{\rm b,mean}}. \tag{26}$$

Then, by denoting $E_{\rm hvac}$ as the total HVAC energy consumption during a complete VB cycle, and $E_{\rm b}$ as the total HVAC energy consumption associated with the baseline (i.e., if no VB service is provided), we can determine the relationship between LDR and HVAC energy consumption:

$$\mathrm{LDR}=\frac{\mathrm{AEC}}{P_{\rm hvac,cyc}^{\rm b,mean}\cdot(f-s)}+1=\frac{E_{\rm hvac}}{E_{\rm b}}, \tag{27}$$

which implies that, during a complete VB cycle, if the average VLP changes by a specific percentage relative to the average baseline HVAC power, the total HVAC energy consumption changes by the same percentage compared to the total HVAC energy consumption associated with the baseline.

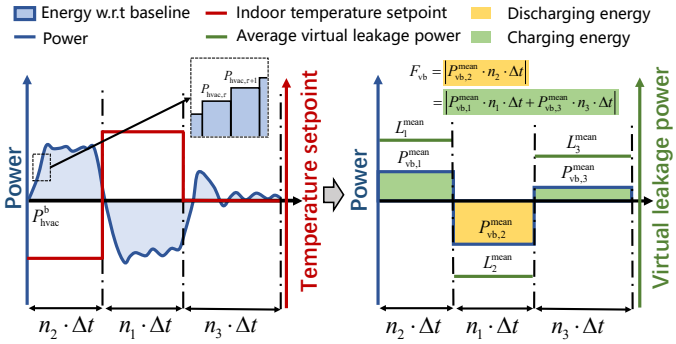

Fig. 2. Relationship between the defined flexibility and HVAC-based VB power variations (using the Up-Down load shifting event as an example).

IV. Optimal Efficiency-Constrained Flexibility Range of HVAC-based VBs

We have shown that the indoor temperature trajectory can be steered to achieve the optimal efficiency of HVAC-based VBs. In this section, we characterize the flexibility of a VB constrained by $\mathrm{AEC} = 0$ and $\mathrm{RTE} = 1$, and present a method to quantify the range of this flexibility. Here, we assume that $\boldsymbol{t_{\mathrm{cyc}}}$ is evenly divided into n_{cyc} time intervals with fixed length Δt. Let T_τ represent the indoor temperature at $t = \tau \cdot \Delta t$, where $\tau = 1, 2, ..., n_{\mathrm{cyc}}$. For each interval $[(\tau-1)\cdot\Delta t, \tau \cdot \Delta t]$, let $P_{\mathrm{hvac},\tau}$ denote the constant power consumption of the HVAC system.

A. VB Flexibility Constrained by the Optimal Efficiency

The analysis in Sections II and III does not presume any specific charging/discharging behaviors (i.e., lengths, sequences or times of charging/discharging) within a complete VB cycle. Still, to align with existing studies and practice, the analysis and method here are based on a type of HVAC-based VB control shown in Fig. 2. It features two equal-length stages for charging and discharging, as well as a final recovery stage returning the indoor temperature to T_{b}. The event of charging (respectively, discharging) and then discharging (respectively, charging) is called "Up-Down" (respectively, "Down-Up").

Thus, a complete VB cycle can be divided into three stages ($n_1+n_2+n_3 = n_{\mathrm{cyc}}$ in Fig. 2). The i-th stage has n_i intervals. Denote T_i^{set} as the indoor temperature setpoint during the i-th stage, and $T_3^{\mathrm{set}} = T_{\mathrm{b}}$. Let τ_i^{s} and τ_i^{f} be the start time index and the final time index of the i-th stage, respectively. Then:

$$\begin{aligned} &\tau_1^{\mathrm{s}} = 1,\ \tau_1^{\mathrm{f}} = n_1; \\ &\tau_2^{\mathrm{s}} = n_1 + 1,\ \tau_2^{\mathrm{f}} = n_1 + n_2; \\ &\tau_3^{\mathrm{s}} = n_1 + n_2 + 1,\ \tau_3^{\mathrm{f}} = n_1 + n_2 + n_3 = n_{\mathrm{cyc}}. \end{aligned} \tag{28}$$

The load shifting ability of an HVAC-based VB can be characterized by the average charging/discharging power in each of the three stages of a complete VB cycle (i.e., $\left[(\tau_i^{\mathrm{s}}-1)\cdot\Delta t, \tau_i^{\mathrm{f}}\cdot\Delta t\right]$, $i = 1, 2, 3$). Therefore, based on (16) and (17), we formulate the average VB power during the i-th stage:

$$\begin{aligned} P_{\mathrm{vb},i}^{\mathrm{mean}} = &-\frac{M\cdot C}{n_i\cdot\Delta t}\left[T_{\mathrm{oa}}\cdot\ln\left(\frac{T_{\tau_i^{\mathrm{f}}}}{T_{\tau_i^{\mathrm{s}}-1}}\right) - (T_{\tau_i^{\mathrm{f}}} - T_{\tau_i^{\mathrm{s}}-1})\right] \\ &+ (L_i^{\mathrm{mean}} - P_{\mathrm{hvac},i}^{\mathrm{b,mean}}), i = 1, 2, 3 \end{aligned} \tag{29}$$

where L_i^{mean} and $P_{\mathrm{hvac},i}^{\mathrm{b,mean}}$ represent the mean $L(t)$ and the mean $P_{\mathrm{hvac}}^{\mathrm{b}}(t)$ during the i-th stage, respectively.

As shown in Fig. 2, for an HVAC-based VB constrained by the optimal efficiency (i.e., $\mathrm{AEC} = 0$ and $\mathrm{RTE} = 1$), we have $\left|P_{\mathrm{vb},2}^{\mathrm{mean}}\cdot n_2\cdot\Delta t\right| = \left|P_{\mathrm{vb},1}^{\mathrm{mean}}\cdot n_1\cdot\Delta t + P_{\mathrm{vb},3}^{\mathrm{mean}}\cdot n_3\cdot\Delta t\right|$. Thus, we propose the metric:

$$F_{\mathrm{vb}} = \left|P_{\mathrm{vb},2}^{\mathrm{mean}}\cdot n_2\cdot\Delta t\right| \tag{30}$$

to assess the flexibility of an HVAC-based VB in providing load shifting under the optimal efficiency condition.

B. VB Flexibility Range Constrained by the Optimal Efficiency

It can be inferred from (29) and (30) that, for a given scenario (i.e., for known variations of T_{oa} and $Q_{\mathrm{gain}}(t)$), and assuming that the indoor temperature approaches the new setpoint in time with a well-developed MPC strategy (i.e., $T_{\tau_1^{\mathrm{f}}} = T_1^{\mathrm{set}}$, $T_{\tau_2^{\mathrm{f}}} = T_2^{\mathrm{set}}$, and $T_{\tau_3^{\mathrm{f}}} = T_3^{\mathrm{set}} = T_{\mathrm{b}}$), F_{vb} is determined by the absolute value of $L_2^{\mathrm{mean}} - P_{\mathrm{hvac},2}^{\mathrm{b,mean}}$. Thus, a feasible range of load shifting for an HVAC-based VB constrained by the optimal efficiency can be derived. We refer to this range as the *VB flexibility range* $\left[\underline{F}_{\mathrm{vb}}, \overline{F}_{\mathrm{vb}}\right]$.

An HVAC-based VB's maximum load shifting flexibility, $\overline{F}_{\mathrm{vb}}$, can be obtained by solving:

$$\max \quad (L_2^{\mathrm{mean}} - P_{\mathrm{hvac},2}^{\mathrm{b,mean}})^2 \tag{31a}$$

$$\text{s.t.} \quad \sum_{i=1}^{3}\frac{n_i}{n_{\mathrm{cyc}}}\cdot L_i^{\mathrm{mean}} = P_{\mathrm{hvac,cyc}}^{\mathrm{b,mean}}, \tag{31b}$$

$$\underline{L}_i^{\mathrm{mean}} \le L_i^{\mathrm{mean}} \le \overline{L}_i^{\mathrm{mean}}, i = 1, 2, 3, \tag{31c}$$

where (31b) is a reformulation of the optimal VB efficiency condition (25), and (31c) bounds L_i^{mean} by factors including HVAC power limits, indoor temperature change rate, and feasible region of the temperature trajectory. More details about (31c) are presented in the Appendix. After solving (31), $\overline{F}_{\mathrm{vb}}$ can be computed with (29) and (30).

To obtain $\underline{F}_{\mathrm{vb}}$, we solve the following problem:

$$\begin{aligned} \min \quad & (L_2^{\mathrm{mean}} - P_{\mathrm{hvac},2}^{\mathrm{b,mean}})^2 \\ \text{s.t.} \quad & (31\mathrm{b}), (31\mathrm{c}). \end{aligned} \tag{32}$$

In general, the range of L_2^{mean} for ensuring $\mathrm{AEC} = 0$ and $\mathrm{RTE} = 1$, which is a subset of $\left[\underline{L}_2^{\mathrm{mean}}, \overline{L}_2^{\mathrm{mean}}\right]$, can be obtained by solving (31) and (32). The HVAC-based VB's load shifting flexibility range, $\left[\underline{F}_{\mathrm{vb}}, \overline{F}_{\mathrm{vb}}\right]$, then can be computed with (29) and (30). Any F_{vb} within this range is feasible and can be achieved by controlling the temperature trajectory to satisfy the corresponding values of L_1^{mean}, L_2^{mean} and L_3^{mean} in the solution, while ensuring $\mathrm{AEC} = 0$ and $\mathrm{RTE} = 1$.

V. Optimal Efficiency-Constrained MPC Control for Providing a Specific Amount of VB Flexibility

After obtaining the flexibility range of an HVAC-based VB, any specific amount of load shifting in this range can be provided. To achieve that, first, the corresponding optimal VLP trajectory (or equivalently, indoor temperature trajectory) is generated. Second, the corresponding optimal HVAC power trajectory, obtained via MPC, is solved.

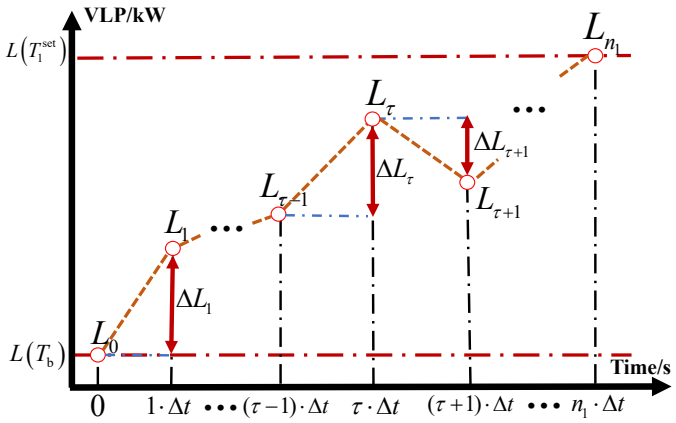

Fig. 3. An example to illustrate the approximated piecewise linear VLP trajectory in the first stage of a complete VB cycle (i.e., $[0, n_1 \cdot \Delta t]$, when the temperature setpoint is decreased from T_b to T_1^{set}).

A. Determining the Trajectory of Virtual Leakage Power

The VLP trajectory $\mathcal{L}_{\mathrm{var}} = \left\{L_0^*, \cdots, L_{n_{\mathrm{cyc}}}^*\right\}$, where L_τ^* is the optimal value of L_τ (explained later), can provide a specific amount of load shifting (i.e., a given value of F_{vb}) while maintaining the optimal efficiency. The determination of this trajectory involves three key steps:

Step 1: Inputting a given F_{vb} to (29) and (30) gives $L_2^{\mathrm{mean},*}$, i.e., the target mean VLP in the second stage of the VB cycle. Then, we obtain $L_1^{\mathrm{mean},*}$ and $L_3^{\mathrm{mean},*}$, i.e., the optimal efficiency-constrained values of L_1^{mean} and L_3^{mean}, by solving:

$$\min \quad \left(\sum_{i=1}^{3} L_i^{\mathrm{mean}} \cdot n_i - P_{\mathrm{hvac,cyc}}^{\mathrm{b,mean}} \cdot n_{\mathrm{cyc}}\right)^2 \tag{33a}$$

$$\text{s.t.} \quad L_2^{\mathrm{mean}} = L_2^{\mathrm{mean},*} \tag{33b}$$

$$\underline{L}_i^{\mathrm{mean}} \le L_i^{\mathrm{mean}} \le \overline{L}_i^{\mathrm{mean}}, i = 1, 3 \tag{33c}$$

where (33a) minimizes the violation of the optimal VB efficiency condition (25), and (33c) is similar to (31c).

Step 2: We next compute the target VLP trajectories for stages 1, 2 and 3 in a VB cycle, based on $L_1^{\mathrm{mean},*}$, $L_2^{\mathrm{mean},*}$, and $L_3^{\mathrm{mean},*}$ obtained in *Step 1*. The relationship between $L(t)$ and $P_{\mathrm{hvac}}(t)$ is highly nonlinear and non-convex. Therefore, we approximate the VLP trajectory with a piecewise linear function. Fig. 3 shows an example for the first stage of a complete VB cycle. Let L_τ be the VLP value at time $t = \tau \cdot \Delta t$. Then, the integral of $L(t)$ over the τ-th interval is approximated by $(L_{\tau-1} + L_\tau) \cdot \Delta t/2$, and the resulting maximum error is $|(L_{\tau-1} - L_\tau) \cdot \Delta t/2|$ since $L(t)$ is monotonic in each interval (which is implied by (1), (10) and (11)). For commercial buildings, the change magnitude of the VLP in each interval (i.e., $|L_{\tau-1} - L_\tau|$) is relatively small, so when Δt conforms to a certain range, the error caused by the approximation can be ignored. The effectiveness of the proposed method is demonstrated in Section VI.

Let $\mathcal{L}_{\mathrm{var},i} = \left\{L_{\tau_i^{\mathrm{s}}}^*, \cdots, L_{\tau_i^{\mathrm{f}}}^*\right\}$ be the target VLP trajectory for the i-th stage of a VB cycle. It is obtained by solving:

$$\min \quad \left[\frac{1}{n_i} \cdot \left(\sum_{\tau=\tau_i^{\mathrm{s}}}^{\tau_i^{\mathrm{f}}} \frac{L_{\tau-1} + L_\tau}{2}\right) - L_i^{\mathrm{mean},*}\right]^2 \tag{34a}$$

$$\text{s.t.} \quad L_\tau = L_{\tau_i^{\mathrm{s}}-1} + \sum_{k=\tau_i^{\mathrm{s}}}^{\tau} \Delta L_k, \tau = \tau_i^{\mathrm{s}}, \cdots, \tau_i^{\mathrm{f}} \tag{34b}$$

$$\underline{\Delta L}_\tau \le \Delta L_\tau \le \overline{\Delta L}_\tau, \tau = \tau_i^{\mathrm{s}}, \cdots, \tau_i^{\mathrm{f}} \tag{34c}$$

$$\underline{L}_\tau \le L_\tau \le \overline{L}_\tau, \tau = \tau_i^{\mathrm{s}}, \cdots, \tau_i^{\mathrm{f}} \tag{34d}$$

$$L_{\tau_1^{\mathrm{s}}-1} = L(T_\mathrm{b}), L_{\tau_1^{\mathrm{f}}} = L(T_1^{\mathrm{set}}) \tag{34e}$$

$$L_{\tau_2^{\mathrm{s}}-1} = L(T_1^{\mathrm{set}}), L_{\tau_2^{\mathrm{f}}} = L(T_2^{\mathrm{set}}) \tag{34f}$$

$$L_{\tau_3^{\mathrm{s}}-1} = L(T_2^{\mathrm{set}}), L_{\tau_3^{\mathrm{f}}} = L(T_\mathrm{b}), \tag{34g}$$

where ΔL_τ is the value of VLP increment at the τ-th time interval (see Fig. 3) and $L(T_\mathrm{b})$, $L(T_1^{\mathrm{set}})$, and $L(T_2^{\mathrm{set}})$ are the VLP values corresponding to T_b, T_1^{set}, and T_2^{set}, respectively. The objective function (34a) makes the mean value of $\mathcal{L}_{\mathrm{var},i}$ approach the target value $L_i^{\mathrm{mean},*}$; (34b) expresses the variation of L_τ; (34c) and (34d) ensure that the VLP trajectory, constrained by power and other limits, can be achieved (more details are in the Appendix); (34e), (34f) and (34g) define boundary conditions for the problems associated with the first, second, and third stages of a VB cycle, respectively.

Step 3: Finally, we obtain VLP variations over the complete VB cycle:

$$\mathcal{L}_{\mathrm{var}} = \mathcal{L}_{\mathrm{var},1} \cup \mathcal{L}_{\mathrm{var},2} \cup \mathcal{L}_{\mathrm{var},3} = \left\{L_0^*, \cdots, L_{n_{\mathrm{cyc}}}^*\right\}. \tag{35}$$

B. Determining MPC-based HVAC Power Variations

We develop an MPC method to determine the HVAC power trajectory, so that the mean VLP in each time interval $[(\tau-1)\cdot\Delta t, \tau\cdot\Delta t]$ approaches $(L_{\tau-1}^* + L_\tau^*)/2$. In this way, the VB provides the targeted amount of load shifting (i.e., the given value of F_{vb}), while ensuring $\mathrm{AEC} = 0$ and $\mathrm{RTE} = 1$.

Let $T_{\tau-1}^{\mathrm{mea}}$ and $L_{\tau-1}^{\mathrm{mea}}$ be the measured indoor temperature and corresponding VLP value at the previous time step $t = (\tau-1)\cdot\Delta t$, respectively. The MPC is implemented by solving the following problem that determines $P_{\mathrm{hvac},\tau}$, i.e., HVAC power in the next time interval:

$$\min \quad \left(\frac{L_{\tau-1}^{\mathrm{mea}} + \tilde{L}_\tau}{2} - \frac{L_{\tau-1}^* + L_\tau^*}{2}\right)^2 \tag{36a}$$

$$\text{s.t.} \quad \tilde{L}_\tau = \frac{\tilde{T}_{\mathrm{oa},\tau} - \tilde{T}_\tau}{R \cdot COP} + \frac{1}{COP} \cdot Q_{\mathrm{gain}}(\tau \cdot \Delta t) \tag{36b}$$

$$P_{\mathrm{hvac},\tau} = -M \cdot C \cdot \frac{\tilde{T}_\tau - T_{\tau-1}^{\mathrm{mea}}}{COP \cdot \Delta t} + \frac{L_{\tau-1}^{\mathrm{mea}} + \tilde{L}_\tau}{2} \tag{36c}$$

$$P_{\mathrm{hvac}}^{\min} \le P_{\mathrm{hvac},\tau} \le P_{\mathrm{hvac}}^{\max}, \tag{36d}$$

where $\tilde{L}_\tau$ is the predicted VLP, $\tilde{T}_{\mathrm{oa},\tau}$ is the predicted outdoor temperature, and $\tilde{T}_\tau$ is the predicted indoor temperature at $t = \tau \cdot \Delta t$. The Carnot efficiency can not be attained in engineering applications. Thus, we use a constant COP to replace $COP_{\mathrm{carnot}}(T(t))$, as in [1]–[7]. Eqn. (36b) computes the predicted VLP, (36c) specifies the relationship between $P_{\mathrm{hvac},\tau}$ and $\tilde{L}_\tau$ (and, equivalently, $\tilde{T}_\tau$), and (36d) enforces HVAC power limits. By solving (36) in each time step, we obtain $\mathcal{P}_{\mathrm{var}} = \{P_{\mathrm{hvac},1}^*, \cdots, P_{\mathrm{hvac},n_{\mathrm{cyc}}}^*\}$, i.e., an MPC-based HVAC power trajectory over the complete VB cycle, which

This article has been accepted for publication in IEEE Transactions on Power Systems. This is the author's version which has not been fully edited and content may change prior to final publication. Citation information: DOI 10.1109/TPWRS.2025.3596899

TABLE I
THERMAL ZONE AND HVAC PARAMETERS

	Parameter	Value	Parameter	Value
HVAC	β	0.4	T_{sa}	16°C
Thermal zone	C	3.4e3J/°C	C_{w}	5.1e3J/°C
	R_1	1e-5°C/W	R_2	1.3e-3°C/W
Constants	c_{air}	1014.5J/(kg°C)	Δt	60 s

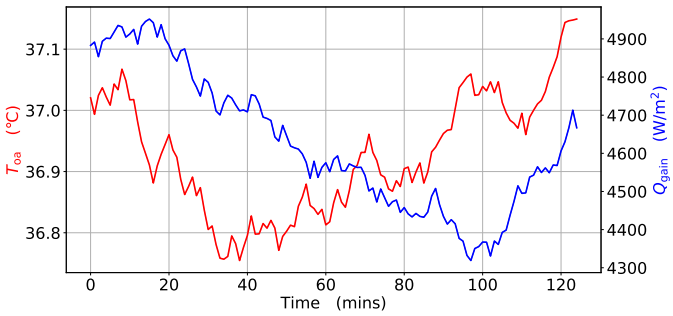

Fig. 4. An example of the outdoor temperature and Q_{gain} used in simulations.

provides the desired amount of load shifting (i.e., the given value of F_{vb}) while keeping $\text{AEC} = 0$ and $\text{RTE} = 1$.

VI. NUMERICAL VERIFICATION

To verify the robustness and effectiveness of our results and methods, we conduct simulations using a more detailed and practical model of buildings and HVAC systems (details in our online Appendix [23]). Assumptions 2 and 3 are also relaxed here. We use the Monte Carlo method to randomly generate 1000 scenarios, which are distinguished by different real-time perturbations (i.e., different time-varying $T_{\text{oa}}(t)$ and $Q_{\text{gain}}(t)$). One example is shown in Fig. 4. We set $T_1^{\text{set}} = 23$ °C, $T_2^{\text{set}} = 21$ °C, $T_3^{\text{set}} = T_{\text{b}} = 22$ °C for Down-Up load shifting events, and $T_1^{\text{set}} = 21$ °C, $T_2^{\text{set}} = 23$ °C, $T_3^{\text{set}} = T_{\text{b}} = 22$ °C for Up-Down load shifting events. We set $\Delta t = 1$ min. The duration of each stage in a VB cycle is the same. That is, $n_1 = n_2 = n_3 = 30$, and $n_i \cdot \Delta t = 30$ mins for $i = 1, 2, 3$. The building and HVAC system parameters are summarized in Table I.

A. Robustness of the Theoretical Optimal Efficiency Analysis

In this subsection, we use a PI controller to regulate the HVAC power according to the difference between the temperature setpoint and indoor temperature. PI control is a commonly used method in HVAC systems. Therefore, our results represent a simulation of an existing HVAC system, and we use these results to provide the raw data to verify the conclusions from Section III, as well as to serve as a benchmark for us to evaluate the effectiveness of the methods described in Sections IV and V.

For each scenario, both Up-Down and Down-Up events are simulated. All results are shown in Fig. 5. Note that the PI controller does not guarantee that the indoor temperature reaches its setpoint in a specific time period, as perturbations in the simulations are random. Thus, to meet the definition of a complete VB cycle (i.e., Definition 3), in this subsection we

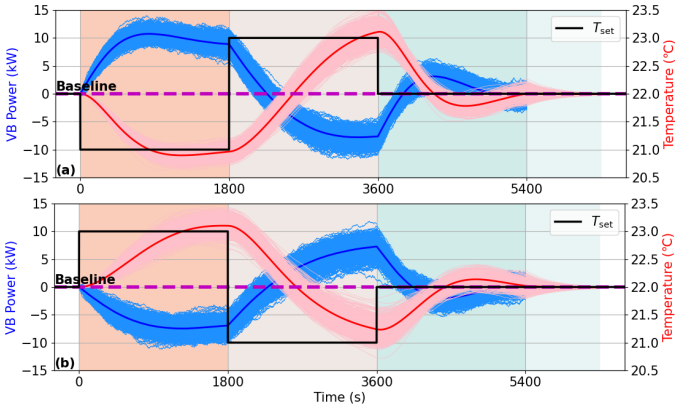

Fig. 5. Results of 2000 simulations: (a) Up-Down; (b) Down-Up.

TABLE II
INDOOR TEMPERATURE TRAJECTORY-DEPENDENT AEC AND RTE ERROR ANALYSIS

Summary Statistics	Maximum	Minimum	Average	Standard Deviation
	0.278%	0.000%	0.018%	3.49×10^{-4}%

	Event Type	RTE	AEC_1 (kWh)	AEC_2 (kWh)	Error
Most Extreme Cases	Up-Down	1.2761	-1.4217	-1.4208	0.063%
		0.5793	2.3234	2.3250	0.072%
	Down-Up	1.1918	-0.9168	-0.9173	0.050%
		0.5813	3.3419	3.3415	0.013%

Note: AEC_1 is calculated by (8), and AEC_2 is calculated by (22); Error is calculated by $|\text{AEC}_1 - \text{AEC}_2|/|\text{AEC}_1| \times 100\%$.

extend the temperature recovery stage (i.e., the third stage in a VB cycle) by 15 mins during which the HVAC power is set to the baseline (i.e, $P_{\text{hvac}}^{\text{b}}$), so that the indoor temperature returns to T_{b} by the end (see the light green area in Fig. 5). This has no impact on the efficiency analysis, as $P_{\text{vb}}(t)$ remains 0 for these 15 mins.

The HVAC-based VB efficiency is affected by the indoor temperature trajectory, as discussed in Section III. Thus, we can use simulated time-series data of indoor temperature and HVAC power (as shown in Fig. 5) to verify the relationship between VB efficiency and indoor temperature trajectory. If such a relationship exists, we can also determine if our computation method (i.e., (22)) accurately quantifies this relationship.

1) Verifying the indoor temperature trajectory-dependent characteristic of VB efficiency: We calculate AEC using two methods: first, using (8) (which is the definition of AEC) based on simulated HVAC power data; second, using (22) (which indicates that the indoor temperature trajectory determines the AEC) using simulated temperature data. If the error between AEC values calculated by these two methods for each event is sufficiently small, the correctness of our derived indoor temperature trajectory-dependent VB efficiency is verified. Table II shows the summary statistics for the percentage error between the two AEC computation methods. The average error is less than 0.02% and so can be neglected even in the most extreme cases. These results demonstrate that, even if Assumptions 2 and 3 are relaxed and the simulation model differs from our theoretical analysis model (1)-(4), our analysis

This article has been accepted for publication in IEEE Transactions on Power Systems. This is the author's version which has not been fully edited and content may change prior to final publication. Citation information: DOI 10.1109/TPWRS.2025.3596899

TABLE III
VERIFICATION OF THE OPTIMAL EFFICIENCY CONDITION

Event Type	RTE	$\int P^{\mathrm{b}}_{\mathrm{hvac}}(t)\cdot dt$ (=E_{hvac}, kWh)	E_{c} (kWh)	E_{d} (kWh)	LDR
Up-Down	0.9994	83.668	54.95	54.91	1.0011
	0.9999	83.665	59.71	59.70	1.0010
	1.0008	83.487	59.04	59.09	0.9989
	1.0001	83.504	56.55	56.55	0.9991
	0.9993	83.668	56.00	55.96	1.0011
Down-Up	0.9992	83.670	61.89	61.84	1.0011
	0.9999	83.665	56.36	56.35	1.0010
	1.0007	83.480	54.38	54.42	0.9988
	1.0000	83.615	60.59	60.59	1.0004

of the impact of indoor temperature trajectory on HVAC-based VB efficiency remains robust, and this impact can be accurately quantified by the proposed VLP based method.

2) Verifying the optimal efficiency condition: We further analyze the existence of specific indoor temperature trajectories that make the VB exhibit the optimal efficiency ($\mathrm{AEC}=0$ and $\mathrm{RTE}=1$). Out of 2000 simulations, 9 events achieve nearly the optimal VB efficiency (i.e., $1-10^{-3}<\mathrm{RTE}<1+10^{-3}$, where we allow a small numerical error tolerance). We also calculate the LDR (as shown by (26), LDR quantifies the difference between the average VLP and average baseline HVAC power, i.e., the deviation from the optimal VB efficiency condition). Considering numerical errors, we assume $1-10^{-3}<\mathrm{LDR}<1+10^{-3}$ achieves the optimal efficiency condition. Results are shown in Table III. In these events, $\mathrm{LDR}=1$ corresponds to $\mathrm{RTE}=1$, and vice versa. The results verify the correctness of the optimal VB efficiency condition, stating that an HVAC-based VB exhibits $\mathrm{RTE}=1$ (and equivalently, $\mathrm{AEC}=0$) if and only if the integrals of the VLP and the baseline HVAC power over the complete VB cycle are the same.

3) Efficiency loss caused by violating the optimal efficiency condition: We also examine the impact of different indoor temperature trajectories on VB efficiency. Fig. 6 quantifies the efficiency loss caused by indoor temperature trajectories that are not constrained by the optimal efficiency condition (i.e., $\mathrm{LDR}\neq 1$). As shown in Fig. 6(a), the Pearson correlation coefficient (r) between LDR and $(E_{\mathrm{b}}+\mathrm{AEC})/E_{\mathrm{b}}$ ($=E_{\mathrm{hvac}}/E_{\mathrm{b}}$, i.e., the HVAC energy consumption when providing load shifting relative to the baseline consumption) is 0.99999. This verifies (27); that is, an unconstrained indoor temperature trajectory results in $\mathrm{LDR}\neq 1$, and further leads to inefficient behavior of HVAC-based VBs. Furthermore, Fig. 6(b) illustrates an approximately linear relationship between LDR and RTE. Specifically, a 1% increase in the average VLP relative to the average baseline HVAC power results in a nearly 10% decrease of the RTE (or equivalently, a nearly 10% decrease in E_{d} relative to E_{c}; see (7)). That is, a slight change in the VLP variation (or equivalently, the indoor temperature trajectory) within the VB cycle significantly influences the efficiency.

4) Applicability to Multi-Zone Commercial Buildings: To simplify the derivation in Section III, the entire commercial building is modeled as a single-zone equivalent system. When extending this analysis to an individual zone within a multi-zone commercial building, the primary distinction lies in the presence of inter-zone heat transfer. For each zone, this inter-zone heat transfer can be incorporated into the term Q_{gain}. Since Q_{gain} is treated as an arbitrary input in our theoretical analysis, the inclusion of these heat transfer terms does not alter the analytical results. Therefore, the theoretical conclusions derived from the single-zone model remain valid for each zone in a multi-zone building, provided that inter-zone heat transfer is appropriately accounted for in Q_{gain}. Furthermore, when analyzing the overall energy efficiency of a multi-zone commercial building participating in DR services, there are two possible approaches. One approach is to aggregate the results obtained from analyzing each individual zone. Alternatively, the overall VLP of the building can be determined by first calculating the average temperature of the entire building, where the temperatures of all zones are weighted according to their respective thermal capacitances. Although an analytical explanation for the second approach has not yet been established, our simulation results demonstrate its correctness and feasibility. Specifically, we conducted 2000 VB simulations on a two-zone HVAC system, where each zone is modeled as a 2R2C network, as illustrated in Fig. 7. The simulation results consistently show that, within any VB cycle, the integral of the overall VLP is equal to the total additional energy consumption, i.e., $\mathrm{AEC}=\int\left[L(t)-P^{\mathrm{b}}_{\mathrm{hvac}}(t)\right]\cdot dt$ (or equivalently, $\mathrm{LDR}=(E_{\mathrm{b}}+\mathrm{AEC})/E_{\mathrm{b}}$).

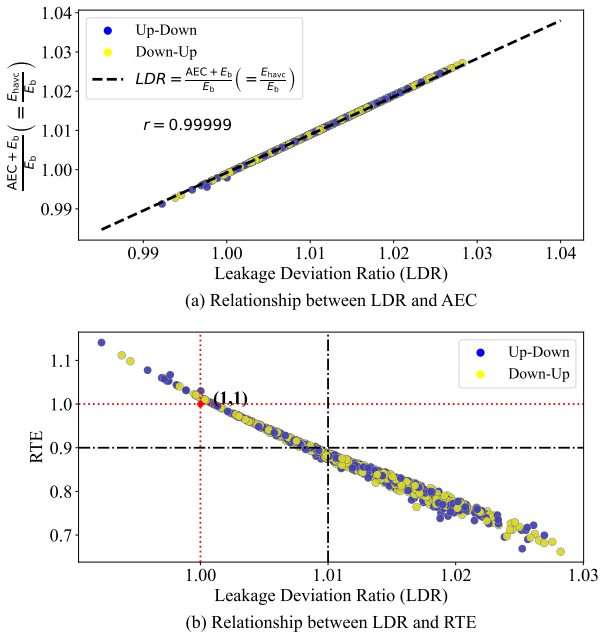

(a) Relationship between LDR and AEC

(b) Relationship between LDR and RTE

Fig. 6. The relationship between HVAC-based VB efficiency and the optimal efficiency condition.

B. Effectiveness of Quantifying the Optimal Efficiency-Constrained Flexibility Range

The load shifting flexibility ranges of the HVAC-based VB in 1000 scenarios are quantified using the method in Section IV. The results are shown in Fig. 8. In each scenario, $P^{\mathrm{b,mean}}_{\mathrm{hvac,cyc}}$ varies, causing changes to the flexibility

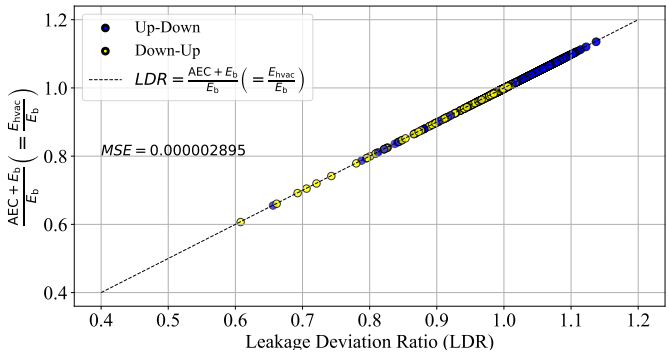

Fig. 7. Verification of the optimal efficiency condition for a two-zone commercial building HVAC system. (The LDR is calculated using the weighted average indoor temperature.)

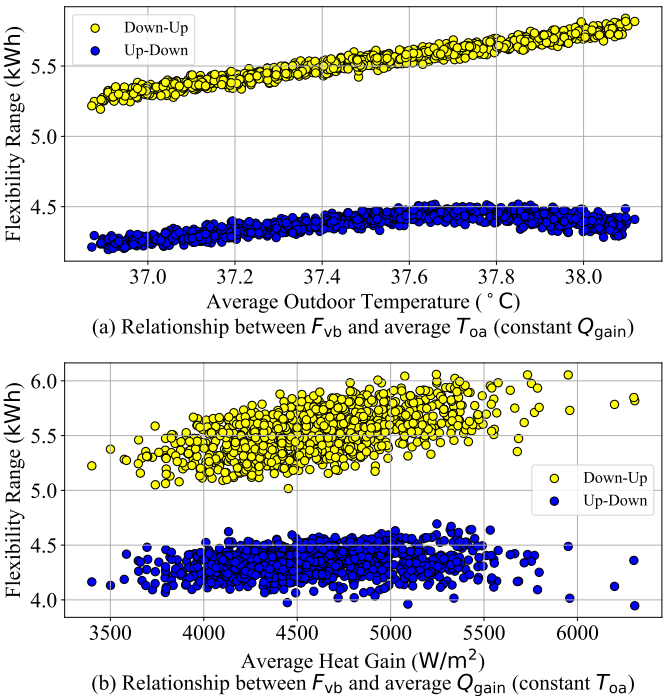

(a) Relationship between F_{vb} and average T_{oa} (constant Q_{gain})

(b) Relationship between F_{vb} and average Q_{gain} (constant T_{oa})

Fig. 8. Load shifting flexibility ranges of the HVAC-based VB under different scenarios.

range $\left[\underline{F}_{\rm vb}, \overline{F}_{\rm vb}\right]$ (which is also affected by variations of $T_{\rm oa}(t)$, $Q_{\rm gain}(t)$, etc.). Interestingly, the Down-Up load shifting flexibility range is typically larger than the Up-Down flexibility range. This is because, in cooling mode, the maximum decreasing rate of indoor temperature is faster than the maximum increasing rate. Thus, the maximum value of $|L_2^{\rm mean} - P_{\rm hvac,2}^{\rm b,mean}|$ for a Down-Up event is greater than that for an Up-Down event. This difference leads to Down-Up events having a larger flexibility range, as $F_{\rm vb}$ is largely determined by $|L_2^{\rm mean} - P_{\rm hvac,2}^{\rm b,mean}|$ (as discussed in Section IV).

Furthermore, the results in Fig. 8 demonstrate that the flexibility range varies across different scenarios. Therefore, we analyze the influence of both $T_{\rm oa}$ and $Q_{\rm gain}$ variations on the flexibility range, using their average values to distinguish between scenarios. Fig. 8 also shows a nearly linear relationship between the flexibility range and the average $T_{\rm oa}$ or $Q_{\rm gain}$.

TABLE IV
PEARSON CORRELATION ANALYSIS OF FLEXIBILITY RANGE AND UNCERTAIN PARAMETERS

Event Types	Parameter	Correlation (r)	P-value	Significance
Up-Down	Avg. $T_{\rm oa}$	0.9796	$< 10^{-10}$	Yes
	Avg. $Q_{\rm gain}$	0.5773	$< 10^{-10}$	Yes
Down-Up	Avg. $T_{\rm oa}$	0.7071	$< 10^{-10}$	Yes
	Avg. $Q_{\rm gain}$	0.1413	$< 10^{-5}$	Yes

Thus, we conduct Pearson correlation analysis (presented in Table IV) to further characterize these relationships across different event types. The analysis reveals distinct patterns in how the flexibility range responds to different uncertain parameters under various event types. Overall, the flexibility range exhibits a higher sensitivity to uncertainties in $T_{\rm oa}$ than to uncertainties in $Q_{\rm gain}$. This sensitivity is especially pronounced in Up-Down events, where the flexibility range is strongly influenced by changes in $T_{\rm oa}$, while its response to $Q_{\rm gain}$ is more moderate. For Down-Up events, the flexibility range still shows some sensitivity to $T_{\rm oa}$, but its dependence on $Q_{\rm gain}$ becomes even weaker. These results indicate that, regardless of event type, $T_{\rm oa}$ is the primary factor affecting the flexibility range, whereas the impact of $Q_{\rm gain}$ is relatively limited. Moreover, the degree of sensitivity to these uncertainties varies between event types, with Up-Down events generally exhibiting greater overall sensitivity than Down-Up events. All observed trends are statistically significant.

C. Effectiveness of Providing a Specific Amount of Load Shifting Constrained by the Optimal Efficiency Condition

To test our MPC method, for each scenario, we implement it 100 times, each providing a specific amount of Up-Down or Down-Up load shifting within the flexibility range. Fig. 9 shows the power variations and indoor temperature trajectories under one scenario. First, the proposed MPC controller effectively responds to setpoint changes and ensures that the temperature reaches the new setpoint in time. Second, as shown in Fig. 10, for both Down-Up and Up-Down events, our MPC method achieves RTE values that are always within $[1 - 1.0 \times 10^{-4}, 1 + 1.0 \times 10^{-4}]$. That is, the proposed MPC method is able to provide a required amount of load shifting while maintaining the optimal efficiency.

D. Implications of Imprecise Building Parameters

The principal challenge in implementing the proposed approach is the difficulty in acquiring the precise parameters needed for the VLP formula, since accurate building characteristics are often hard to obtain in specific commercial buildings. Nevertheless, we have observed that VLP decreases monotonically with increasing indoor temperature. Consequently, the optimal efficiency condition, $L_{\rm cyc}^{\rm mean} = P_{\rm hvac,cyc}^{\rm b,mean}$, can be approximated by maintaining the average indoor temperature ($\int_s^f T(t) \cdot dt/(f-s)$) close to the

This article has been accepted for publication in IEEE Transactions on Power Systems. This is the author's version which has not been fully edited and content may change prior to final publication. Citation information: DOI 10.1109/TPWRS.2025.3596899

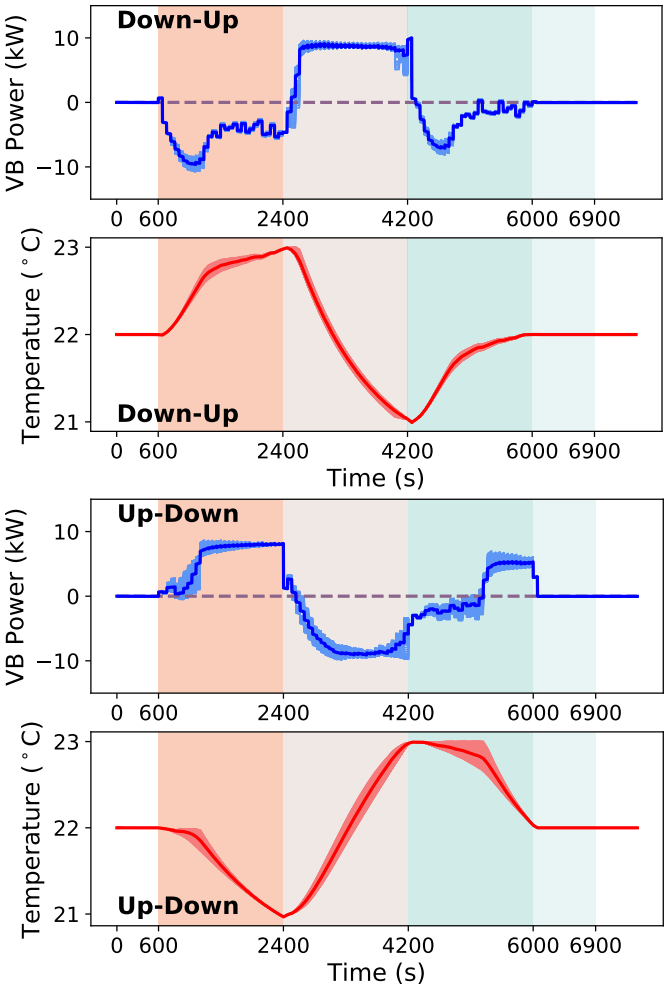

Fig. 9. Trajectories of the HVAC power and indoor temperature, corresponding to events using our MPC method to provide specific amounts of load shifting while ensuring RTE $= 1$ and AEC $= 0$.

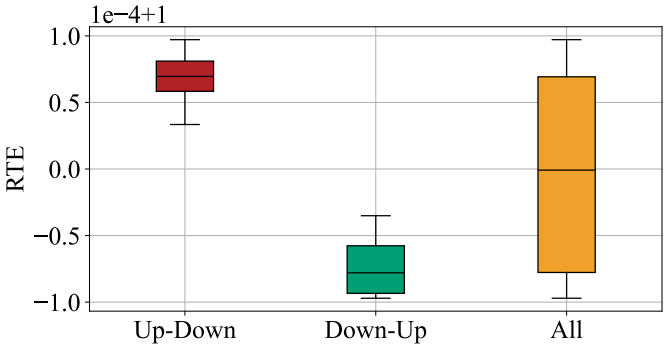

Fig. 10. Statistics of the VB's efficiency, corresponding to events using our MPC method to provide specific amounts of load shifting.

baseline temperature (T_b) during the DR period. As illustrated in Fig. 11, our analysis of the relationship between $\left[\int_s^f T(t)\cdot dt/(f-s)\right]/T_\mathrm{b}$ and $E_\mathrm{hvac}/E_\mathrm{b}$ reveals that when the optimal efficiency ($E_\mathrm{hvac}/E_\mathrm{b}=1$) is achieved, the ratio $\left[\int_s^f T(t)\cdot dt/(f-s)\right]/T_\mathrm{b}$ remains within a narrow range of 1 ± 0.006. This finding suggests that regulating the average

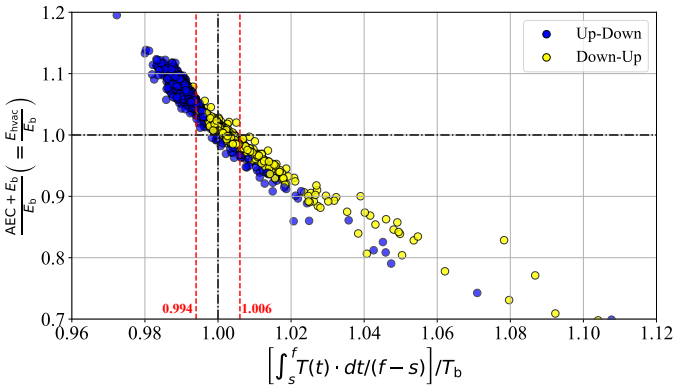

Fig. 11. Relationship between AEC and the ratio of average indoor temperature to baseline indoor temperature.

indoor temperature during DR events can effectively ensure optimal efficiency, even without access to the precise parameters needed for the VLP formula.

VII. Conclusions

For HVAC-based VBs participating in DR, our theoretical analysis showed that the indoor temperature trajectory over a complete VB cycle is a key factor impacting energy efficiency. A novel concept called VLP and a method based upon that were proposed to quantify this impact. Furthermore, based on the VLP trajectory, we derived the condition for a VB to achieve the optimal efficiency (RTE $= 1$ and AEC $= 0$). Then, we developed a method for computing the load shifting flexibility range of the VB constrained by the optimal efficiency condition. We also proposed an MPC approach to provide a given amount of load shifting while meeting the optimal efficiency condition. The robustness and effectiveness of our analysis and methods are verified by numerical simulations.

Appendix
Details on the Bounds of L_τ, ΔL_τ, and L_i^mean

Variables L_τ, ΔL_τ and L_i^mean are generally bounded by power limits of the HVAC system. As mentioned in Section V, the coefficient of performance is assumed to be a constant COP, and the dynamics of T_τ and L_τ caused by $P_{\mathrm{hvac},\tau}$ can be described by:

$$L_\tau = \frac{T_\mathrm{oa}-T_\tau}{R\cdot COP}+\frac{1}{COP}\cdot Q_\mathrm{gain}(\tau\cdot\Delta t), \tag{37a}$$

$$P_{\mathrm{hvac},\tau} = -M\cdot C\cdot\frac{T_\tau-T_{\tau-1}}{COP\cdot\Delta t}+\frac{L_{\tau-1}+L_\tau}{2}. \tag{37b}$$

Therefore, we can obtain the range of the indoor temperature trajectories first. Then, the bounds of L_τ and L_i^mean (i.e., the range of the VLP trajectories) can be calculated.

Considering a stage where the temperature setpoint is decreased during a complete VB cycle, Algorithm A.1 shows the detailed process of computing the range of indoor temperature trajectories and the bounds of the average VLP ($\overline{L}_i^\mathrm{mean}$ and $\underline{L}_i^\mathrm{mean}$). The method of computing the bounds for a stage where the temperature setpoint is increased is similar to Algorithm A.1.

Algorithm A.1 Computing the bounds of L_τ and L_i^{mean} throughout a stage where the temperature setpoint is decreased

INPUT: start temperature $T_{\tau_i^{\text{s}}-1}$ and final temperature $T_{\tau_i^{\text{f}}}$ (corresponding to indoor temperature setpoints).

1). Find the upper bounds of L_i^{mean} and L_τ:

$\underline{T}_{\tau_i^{\text{s}}-1} \leftarrow T_{\tau_i^{\text{s}}-1}$

$\overline{L}_{\tau_i^{\text{s}}-1} \leftarrow L(\underline{T}_{\tau_i^{\text{s}}-1})$

$P_{\text{hvac},\tau_i^{\text{s}}} \leftarrow P_{\text{hvac}}^{\max}$

for $\tau = \tau_i^{\text{s}}, \tau_i^{\text{s}}+1, ..., \tau_i^{\text{f}}$ **do**

  Estimate T_τ by solving (37) based on $P_{\text{hvac},\tau}$ and $\underline{T}_{\tau-1}$

  if $T_\tau \le T_{\tau_i^{\text{f}}}$ **then**

    $P_{\text{hvac},\tau+1} \leftarrow L(T_{\tau_i^{\text{f}}})$

    $\underline{T}_\tau \leftarrow T_{\tau_i^{\text{f}}}$

  else

    $P_{\text{hvac},\tau+1} \leftarrow P_{\text{hvac}}^{\max}$

    $\underline{T}_\tau \leftarrow T_\tau$

  end if

  $\overline{L}_\tau \leftarrow L(\underline{T}_\tau)$

end for

$\overline{L}_i^{\text{mean}} \leftarrow \frac{1}{n_i} \sum_{\tau=\tau_i^{\text{s}}}^{\tau_i^{\text{f}}} \overline{L}_\tau$

2). Find the lower bounds of L_i^{mean} and L_τ:

$\overline{T}_{\tau_i^{\text{f}}} \leftarrow T_{\tau_i^{\text{f}}}$

$\underline{L}_{\tau_i^{\text{f}}} \leftarrow L(\overline{T}_{\tau_i^{\text{f}}})$

$P_{\text{hvac},\tau_i^{\text{f}}} \leftarrow P_{\text{hvac}}^{\max}$

for $\tau = \tau_i^{\text{f}}, \tau_i^{\text{f}}-1, ..., \tau_i^{\text{s}}$ **do**

  Estimate $T_{\tau-1}$ by solving (37) based on $P_{\text{hvac},\tau}$ and $\overline{T}_\tau$

  if $T_{\tau-1} \ge T_{\tau_i^{\text{s}}-1}$ **then**

    $P_{\text{hvac},\tau-1} \leftarrow L(T_{\tau_i^{\text{s}}-1})$

    $\overline{T}_{\tau-1} \leftarrow T_{\tau_i^{\text{s}}-1}$

  else

    $P_{\text{hvac},\tau-1} \leftarrow P_{\text{hvac}}^{\max}$

    $\overline{T}_{\tau-1} \leftarrow T_{\tau-1}$

  end if

  $\underline{L}_{\tau-1} \leftarrow L(\overline{T}_{\tau-1})$

end for

$\underline{L}_i^{\text{mean}} \leftarrow \frac{1}{n_i} \sum_{\tau=\tau_i^{\text{s}}}^{\tau_i^{\text{f}}} \underline{L}_\tau$

OUTPUT: $\overline{L}_i^{\text{mean}}, \underline{L}_i^{\text{mean}}, \left\{\overline{L}_{\tau_i^{\text{s}}}, \overline{L}_{\tau_i^{\text{s}}+1}, \cdots, \overline{L}_{\tau_i^{\text{f}}}\right\}$, and $\left\{\underline{L}_{\tau_i^{\text{s}}}, \underline{L}_{\tau_i^{\text{s}}+1}, \cdots, \underline{L}_{\tau_i^{\text{f}}}\right\}$.

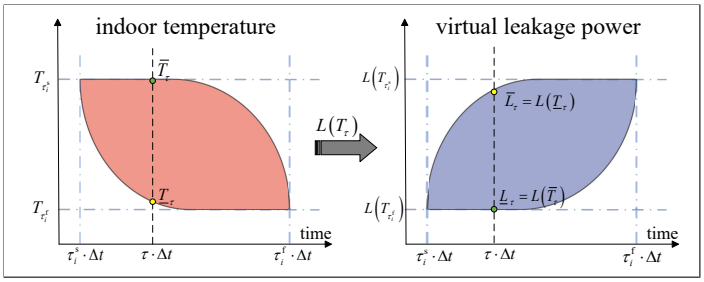

Fig. A.1. Feasible ranges of the indoor temperature trajectories and the corresponding VLP trajectories throughout the i-th stage in a complete VB cycle. (In this example, a temperature setpoint decrease is assumed for this stage.)

After implementing the algorithm, we obtain a region containing all possible indoor temperature trajectories that may be observed in this stage of the VB cycle, and a feasible region for VLP trajectories (as shown in Fig. A.1). These two regions represent the limits of T_τ and L_τ variations during each time interval $[(\tau-1)\cdot\Delta t, \tau\cdot\Delta t]$.

In addition, the change magnitude of VLP during each time interval, ΔL_τ, is also bounded by the HVAC power limits, and should be constrained in analyzing the VLP trajectory (or equivalently, the indoor temperature trajectory). The slight difference between $Q_{\text{gain}}((\tau-1)\cdot\Delta t)$ and $Q_{\text{gain}}(\tau\cdot\Delta t)$ can be ignored, as the variation of $Q_{\text{gain}}(t)$ is slow and small within such a short interval. Therefore, based on (37), the relationship between ΔL_τ and $P_{\text{hvac},\tau}$ can be represented as:

$$\Delta L_\tau = \frac{2\cdot\Delta t}{2\cdot M\cdot C\cdot R + \Delta t}\cdot\left(P_{\text{hvac},\tau} - L_{\tau-1}\right). \tag{38}$$

This means that the value of ΔL_τ increases with $P_{\text{hvac},\tau}$ and decreases with $L_{\tau-1}$. As both $P_{\text{hvac},\tau}$ and $L_{\tau-1}$ are defined to be positive, the bounds of ΔL_τ can be calculated by:

$$\overline{\Delta L}_\tau = \frac{\left(P_{\text{hvac}}^{\max} - \underline{L}_{\tau-1}\right)\cdot 2\cdot\Delta t}{2\cdot M\cdot C\cdot R + \Delta t}, \tag{39a}$$

$$\underline{\Delta L}_\tau = \frac{\left(P_{\text{hvac}}^{\min} - \overline{L}_{\tau-1}\right)\cdot 2\cdot\Delta t}{2\cdot M\cdot C\cdot R + \Delta t}. \tag{39b}$$

ACKNOWLEDGMENTS

The authors would like to thank Prof. Ian Hiskens with the University of Michigan for valuable discussions.

REFERENCES

[1] G. Tian, S. Faddel, Q. Zhou, Z. Qu, and A. Parlato, "Optimal coordination of HVAC scheduling for commercial buildings," in *2020 IEEE Texas Power and Energy Conference (TPEC)*. IEEE, 2020, pp. 1–5.

[2] G. Tian, Q. Z. Sun, and W. Wang, "Real-time flexibility quantification of a building HVAC system for peak demand reduction," *IEEE Transactions on Power Systems*, vol. 37, no. 5, pp. 3862–3874, 2021.

[3] W. Wang, G. Tian, Q. Z. Sun, and H. Liu, "A control framework to enable a commercial building hvac system for energy and regulation market signal tracking," *IEEE Transactions on Power Systems*, vol. 38, no. 1, pp. 290–301, 2022.

[4] S. Lu, W. Gu, S. Ding, S. Yao, H. Lu, and X. Yuan, "Data-driven aggregate thermal dynamic model for buildings: A regression approach," *IEEE Transactions on Smart Grid*, vol. 13, no. 1, pp. 227–242, 2021.

[5] J. T. Hughes, A. D. Domínguez-García, and K. Poolla, "Identification of virtual battery models for flexible loads," *IEEE Transactions on Power Systems*, vol. 31, no. 6, pp. 4660–4669, 2016.

[6] Y. Lin, P. Barooah, S. Meyn, and T. Middelkoop, "Experimental evaluation of frequency regulation from commercial building HVAC systems," *IEEE Transactions on Smart Grid*, vol. 6, no. 2, pp. 776–783, 2015.

[7] J. S. MacDonald, E. Vrettos, and D. S. Callaway, "A critical exploration of the efficiency impacts of demand response from HVAC in commercial buildings," *Proceedings of the IEEE*, vol. 108, no. 9, pp. 1623–1639, 2020.

[8] S. Córdova, Á. Lorca, D. E. Olivares *et al.*, "Aggregate modeling of thermostatically controlled loads for microgrid energy management systems," *IEEE Transactions on Smart Grid*, 2023.

[9] I. Beil, I. Hiskens, and S. Backhaus, "Round-trip efficiency of fast demand response in a large commercial air conditioner," *Energy and Buildings*, vol. 97, pp. 47–55, 2015.

[10] A. Keskar, D. Anderson, J. X. Johnson, I. A. Hiskens, and J. L. Mathieu, "Do commercial buildings become less efficient when they provide grid ancillary services?" *Energy Efficiency*, vol. 13, pp. 487–501, 2020.

[11] A. Keskar, S. Lei, T. Webb, S. Nagy, I. A. Hiskens, J. L. Mathieu, and J. X. Johnson, "Assessing the performance of global thermostat adjustment in commercial buildings for load shifting demand response," *Environmental Research: Infrastructure and Sustainability*, vol. 2, no. 1, p. 015003, Mar. 2022.
[12] N. S. Raman and P. Barooah, "Analysis of round-trip efficiency of an HVAC-based virtual battery," 2018.
[13] G. Goddard, J. Klose, and S. Backhaus, "Model development and identification for fast demand response in commercial HVAC systems," *IEEE Transactions on Smart Grid*, vol. 5, no. 4, pp. 2084–2092, 2014.
[14] E. Vrettos, E. C. Kara, J. MacDonald, G. Andersson, and D. S. Callaway, "Experimental demonstration of frequency regulation by commercial buildings—part i: Modeling and hierarchical control design," *IEEE Transactions on Smart Grid*, vol. 9, no. 4, pp. 3213–3223, 2016.
[15] ——, "Experimental demonstration of frequency regulation by commercial buildings—part ii: Results and performance evaluation," *IEEE Transactions on Smart Grid*, vol. 9, no. 4, pp. 3224–3234, 2016.
[16] Y. Lin, J. L. Mathieu, J. X. Johnson, I. A. Hiskens, and S. Backhaus, "Explaining inefficiencies in commercial buildings providing power system ancillary services," *Energy and Buildings*, vol. 152, pp. 216–226, 2017.
[17] Y. Lin, P. Barooah, and J. L. Mathieu, "Ancillary services through demand scheduling and control of commercial buildings," *IEEE Transactions on Power Systems*, vol. 32, no. 1, pp. 186–197, 2016.
[18] N. S. Raman and P. Barooah, "On the round-trip efficiency of an HVAC-based virtual battery," *IEEE Transactions on Smart Grid*, vol. 11, no. 1, pp. 403–410, 2019.
[19] R. Kramer, J. Van Schijndel, and H. Schellen, "Simplified thermal and hygric building models: A literature review," *Frontiers of architectural research*, vol. 1, no. 4, pp. 318–325, 2012.
[20] Y. A. Cengel, M. A. Boles, and M. Kanoğlu, *Thermodynamics: an engineering approach*. McGraw-hill New York, 2011, vol. 5.
[21] L.-a. Ying, *Infinite element methods*. Springer, 1995.
[22] J. A. C. Weideman, "Numerical integration of periodic functions: A few examples," *The American mathematical monthly*, vol. 109, no. 1, pp. 21–36, 2002.
[23] "Appendix of paper: Energy efficiency in commercial HVAC-based virtual batteries for load shifting: Theoretical analysis and enhancement," online, available: https://drive.google.com/file/d/1CLd9Kh0IftN3INmAvb6C0eF0k4WkY4PR/view?usp=sharing.

Weimin Wu (Student Member, IEEE) received the B.E. degree in energy and power engineering from Soochow University, Suzhou, China, in 2022. He is currently pursuing the Ph.D. degree in energy science and engineering with The Chinese University of Hong Kong (Shenzhen), Shenzhen, China. His research interests include power system decarbonization and power-transportation coupled systems.

Shunbo Lei (Senior Member, IEEE) received the B.E. degree in electrical engineering from Huazhong University of Science and Technology, Wuhan, China, in 2013, and the Ph.D. degree in electrical engineering from The University of Hong Kong, Hong Kong SAR, China, in 2017. He was a Visiting Scholar with Argonne National Laboratory, Lemont, IL, USA, from 2015 to 2017, a Postdoctoral Researcher with The University of Hong Kong from 2017 to 2019, and a Research Fellow with the University of Michigan, Ann Arbor, MI, USA, from 2019 to 2021. He is currently an Assistant Professor and a Presidential Young Fellow with the School of Science and Engineering, The Chinese University of Hong Kong, Shenzhen, China. His research interests include power systems, resilience, grid-interactive buildings, optimization, and learning.

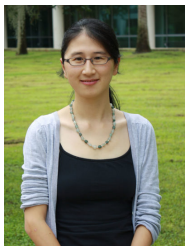

Qun Zhou Sun (Member, IEEE) received the Ph.D. degree in electrical engineering from Iowa State University, Ames, IA, USA, in 2011. She is an Associate Professor with the University of Central Florida (UCF), Orlando, FL, USA. She is the Director of UCF Smart Infrastructure Data Analytics Lab. Before joining UCF, she worked for Genscape and GE Grid Solutions as a Power System Engineer. Her research interests include grid-edge resources, including smart buildings, rooftop PVs, and batteries, and their interactions with the grid. She is dedicated to the research that improves energy sustainability, resiliency, and security. Her research leverages advanced data analytics and probabilistic algorithms to enhance energy efficiency and security.

Johanna L. Mathieu (Senior Member, IEEE) received the B.S. degree in ocean engineering from the Massachusetts Institute of Technology, Cambridge, MA, USA, in 2004, and the M.S. and Ph.D. degrees in mechanical engineering from the University of California at Berkeley, Berkeley, USA, in 2008 and 2012, respectively. She is an Associate Professor with the Department of Electrical Engineering and Computer Science, University of Michigan, Ann Arbor, MI, USA. Prior to joining the University of Michigan, she was a Postdoctoral Researcher with the Swiss Federal Institute of Technology (ETH) Zurich, Switzerland. Her research interests include modeling, estimation, control, and optimization of distributed energy resources.